

Analysis of Metronidazole Adsorption onto Cellulose-Chitosan Composite Adsorbent

Chukwunonso O. Aniagor*, Matthew C. Menkiti*

Department of Chemical Engineering, Nnamdi Azikiwe University, P.M.B. 5025, Awka, Nigeria

*Corresponding Author's E-mail: co.aniagor@unizik.edu.ng; mc.menkiti@unizik.edu.ng

Abstract

In this study composite (Ce-C) was successfully synthesized and further applied for efficient adsorption of metronidazole (MET) molecules from aqueous solutions. Chitosan was doped onto a cellulose substrate with glutaraldehyde as a crosslinking agent to enhance composite durability. The composite exhibited rapid adsorption kinetics, achieving over 90% MET uptake within 80 minutes. Adsorption capacity decreased with increasing temperature due to a possible concentrating of the adsorbate solution, structural changes in the composite and weakening of the cellulose-chitosan linkage. Also, FT-IR analysis confirmed the retention of key functional groups post-adsorption. The BET surface area of 109.64 m²/g and pore diameter of 12.83 nm indicates the presence of relatively large adsorption sites and a mesoporous structure. The Langmuir model and pseudo-first-order model best described the isotherm and kinetics data, respectively. A maximum adsorption capacity (q_{max}) value of 12.72 mg/g was also recorded. Thermodynamic studies showed the process was exothermic ($\Delta H^\circ = -62.27$ kJ/mol) and spontaneous ($\Delta S^\circ = -218.03$ J/Kmol), despite positive Gibbs free energy values. The Ce-C composite also demonstrated excellent reusability with high desorption efficiency across multiple cycles, highlighting its potential as a sustainable, effective adsorbent for removing antibiotic contaminants like MET from wastewater.

Keywords: Adsorption, Composite, Metronidazole, Isotherm, Kinetics, Modelling

1. Introduction

Metronidazole (MET) is an antibiotic commonly used in human and animal therapeutics, particularly for treating bacterial infections (Oba et al., 2021). As a result, it frequently becomes a contaminant in various environments, including households, hospitals, animal husbandry, and wastewater from the agricultural and pharmaceutical industries (Binh et al., 2018). However, unprocessed effluent from the aforementioned environments has led to the release of these MET antibiotics into the aquatic environment. Over time, the presence of these active antibiotic components in multiple water bodies has been reported, with concentrations ranging from 50 - 100 ng/L (Papageorgiou et al., 2024). The threat posed by antibiotic pollution to both the environment and human health cannot be over-emphasized. Inyinbor et al. (2018) reported that antibiotic bioaccumulation led to reproductive issues in fish, including the feminization of male fish. Additionally, the environmental risks associated with the emergence of antibiotic-resistant genes and bacteria remain a persistent concern (Koch et al., 2021). As noted by Hejna et al. (2022) and Khan and Barros (2023), the implications of MET contamination suggest both immediate and long-term negative ecological and environmental impacts. Therefore, there is a strong imperative to efficiently remove MET antibiotics from wastewater.

The issue of environmental pollution by antibiotics has been addressed using well-known techniques such as nanofiltration, electrolysis, reverse osmosis, ion exchange, chemical disinfection, and oxidation (Abd El-Monaem et al., 2022; Ferrah et al., 2022; Mashile & Nomngongo, 2021). These techniques are often bedeviled by several drawbacks such as operational high cost, fouling and use of non-ecofriendly chemical precursors that harm the environment (Kumar et al., 2022). Due to its cost-effectiveness, adsorbent reusability, process flexibility and improved treatment efficiency, adsorption is a preferred water treatment technique (Aniagor et al., 2024). Although

several adsorbents including activated carbon, carbon nanotubes, zeolites, and biochar have been utilized in adsorbing antibiotics from an aqueous environment (Nordin et al., 2023), the performance of renewable biopolymers, such as cellulose and chitosan as wastewater treatment adsorbents are outstanding (Chan et al., 2021). Beyond its structural stabilization role in plants, cellulose is important in various industrial applications due to its sustainability, renewability and eco-friendliness (Wang et al., 2020). Similarly, chitin is a highly crystalline biopolymer whose robust structure is linked to the availability of D-GlcN and D-GlcNAc residues in its structure framework (Iber et al., 2022). To further extend their application and usefulness, cellulose and chitin are often derivatized either via grafting, copolymerization, hydrogel formation, or complexation with other materials to obtain products with improved functional properties (Aniagor et al., 2022).

Luo et al. (2019) incorporated a chitosan/cellulose nanocomposite adsorbent into a porous activated carbon structure using a sol-gel phase inversion method. The nanocomposite product proved successful in adsorbing tylosin antibiotics at low concentrations. Liu et al. (2021) developed a novel adsorbent made from carboxymethyl cellulose, crosslinked chitosan and graphene oxide. The composite was applied to remove sulfamethoxazole and sulfapyridine from wastewater. Gong et al. (2021) used aminated chitosan/cellulose nanocomposite microspheres to adsorb 99.18% of sulfamethoxazole antibiotics from aqueous media. Barus et al. (2022) developed nanocomposite hydrogels from cellulose nanofiber, chitosan, and graphene oxide, which effectively removed methylene blue dye and levofloxacin hemihydrate antibiotic pollutants.

This study, therefore reports the successful use of biopolymeric materials based on cellulose and chitosan for synthesizing an efficient composite (Ce-C). Chitosan was doped onto the cellulose substrate via an in situ adsorption mechanism to obtain a composite polymer with cellulose as the main chain and chitosan oligomers as lateral chains. According to Naebe et al. (2016), the cellulose-chitosan bonding forces have characteristic poor strength. To ensure irreversible adsorption of chitosan on the cellulose substrate, glutaraldehyde was utilized as the crosslinking agent. Therefore, the objectives were (i) to instrumentally characterize the synthesized Ce-C composite (ii) to evaluate how variations in initial MET concentration, adsorbent-adsorbate contact time, and solution temperature influence the ultimate adsorption capacity (iii) to conduct batch adsorption modeling of the experimental equilibrium and kinetics dataset.

2. Materials and methods

2.1. Material collection and sample preparation

Sodium hydroxide, acetic acid, methanol, diethyl ether, hydrochloric acid, and sulfuric acid were procured from the chemical market in Onitsha, Anambra State, Nigeria. Mature jackfruit (*Artocarpus heterophyllus*) peels and periwinkle shells were sourced from a local market in Abagana, Anambra State, Nigeria. The jackfruit fibers were reduced in size, dewaxed by boiling in water, sun-dried to a constant weight, and then ground into fine particles (approximately 50-125 μm). Similarly, the periwinkle shells were washed, sun-dried, pulverized, and ground into fine particles (50-125 μm). Cellulose was extracted from powdered jackfruit fiber through alkali hydrolysis treatment and subsequent bleaching of the hydrolysis product. This was achieved following the methods earlier reported by Merino and Athanassiou (2023). Similarly, the chitin was extracted and deacetylated to obtain chitosan, following the methodology previously described by Ramadhani et al. (2021).

2.2. Fabrication of cellulose–chitosan composite

The cellulose–chitosan (Ce-C) composite was fabricated by solubilizing chitosan powder (10 g) in 100 ml of 2% acetic acid, while 20 g of cellulose powder was separately mixed with 200 ml of distilled water and stirred for 20 min. The chitosan solution and cellulose slurry were combined and stirred for an additional 24 h, with 10 ml of 5% glutaraldehyde added dropwise for crosslinking. The resulting mixture was washed to a neutral pH of 7.0, cast onto a petri dish, and oven-dried at 60°C for 6 h.

2.3. Batch adsorption studies

MET solution of varying concentrations (20-100 mg/L) was prepared and subsequently, a 100 mL volume of adsorbate solution was contacted with 0.5 g of the adsorbent. The setup was agitated at 150 rpm and samples were collected every 5 min until equilibrium. The final adsorbate concentration was determined with a Shimadzu UV-1900 spectrophotometer at ~319 nm and the experimental adsorption capacity was evaluated by Eq. (1).

$$q_e = \frac{(C_0 - C_e) * V}{w} \quad (1)$$

Where initial concentration, final concentration, mass of adsorbent and volume of wastewater id denoted by C_o , C_e , W and V , respectively. Furthermore, the experimental adsorption data were modelled using the dedicated equations presented in Table 1.

Table 1: The adsorption models applied in the study

Model type	Mathematical expression	Eqn No
Isotherm models		
Langmuir	$q_e = \frac{q_m k_L C_e}{1 + k_L C_e}$	(2)
Freundlich	$q_e = K_F (C_e)^{\frac{1}{n_F}}$	(3)
Temkin	$q_e = \frac{RT}{b_T} \ln(K_T C_e)$	(4)
Kinetic models		
Pseudo-first-order	$q_t = q_e [1 - \exp(-k_1 t)]$	(5)
Pseudo-second-order	$q_t = \frac{K_2 q_e^2 t}{1 + K_2 q_e t}$	(6)
Mechanistic models		
Intraparticle diffusion	$q_t = K_{id} \sqrt{t} + C$	(7)
Bangham	$\log \left[\frac{C_o}{C_o - q_t M} \right] = \log \left[\frac{k_b}{2.33 V} \right] + \alpha \log t$	(8)

3. Results and discussion

3.1. Effect of the adsorption process variable

The adsorption capacity of the Ce-C composite for MET was measured over time (0–100 min) at an initial concentration of 40 mg/L. The results showed that the amount of MET adsorbed (q_e , mg/g) increased with contact time, with 92–95% of the maximum adsorption (q_{max}) occurring within the first 70–80 min. This rapid uptake was due to the large number of surface sites available on the adsorbent (Mohamed et al., 2021). Beyond 80 min, the adsorption rate slowed, likely due to ionic repulsion, leading to an equilibrium time of 80 min. The adsorption process was driven by the concentration gradient of MET and contact time. Other studies, such as those by Papageorgiou et al. (2024) and Feng et al. (2022), also noted that maximum adsorption capacity depends on both contact time and initial concentration.

The solution temperature versus adsorption capacity plot as presented in Fig. 1(b) showed a general decrease in the adsorption capacity with rising solution temperature. This is due to the concentration of adsorbate solution, possible degradation of the composite, weakening of the cellulose-chitosan linkage, and solute desorption from the binding site at increasing temperatures. All the aforementioned occurrences ultimately contribute to the observed reduction in adsorption capacity with increasing temperature (Mohamed et al., 2021).

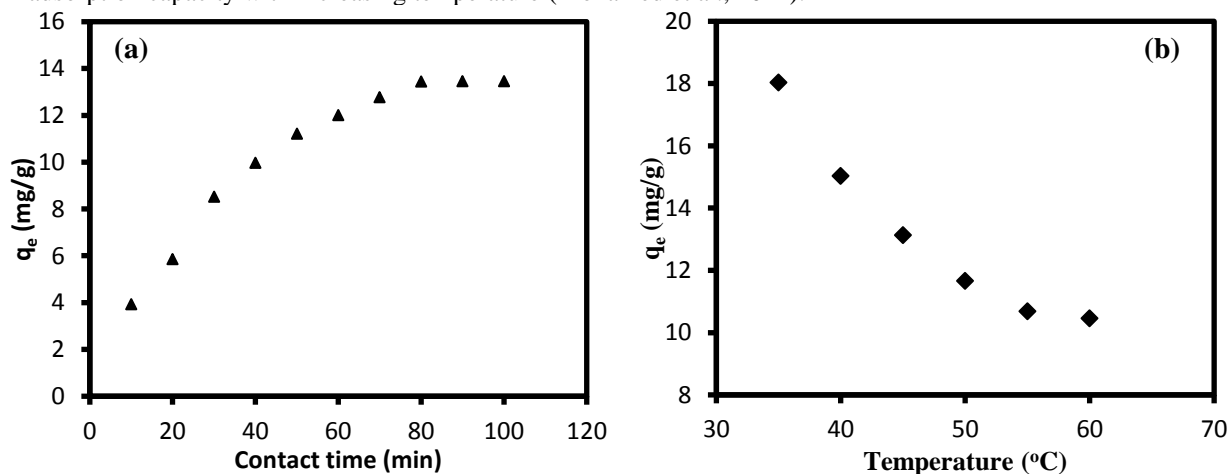


Figure 1: (a) Plot of contact time versus adsorption capacity (q_e) and (b) plot of temperature versus adsorption capacity (q_e)

3.2. Sample characterization results

3.2.1. BET surface area measurement

The result of the BET surface area measurement indicates a specific surface area, pore volume, and pore diameter values of 109.64 m²/g, 0.23 cm³/g, and 12.83 nm, respectively. These results suggest that the Ce-C composite has a relatively high capacity and can accommodate the adsorbed MET molecules (Szentmihályi et al., 2022).

3.2.2. Fourier transform infrared spectroscopy (FTIR) analysis result

The raw Ce-C composite displayed its main functional groups at 3041.76 cm⁻¹ (carboxylic -OH), 2902.14 cm⁻¹ (aliphatic C-H stretching), 1417 cm⁻¹ (NH stretching vibrations), and 700.36 cm⁻¹ (C-O-H twist vibration) (Kumar et al., 2010). The presence of these functional groups confirms that the complexation of cellulose with chitosan does not involve chemical reactions, as the chemical structures of the individual polysaccharides remain unchanged. After adsorption (Fig. 2b), the major functional groups in the raw Ce-C sample were retained, though significant shifts in both wavenumbers and transmittances were observed. Additionally, a -NO₂ group associated with aromatic nitro compounds appeared at 1200.05 cm⁻¹, indicating the presence of adsorbed MET molecules.

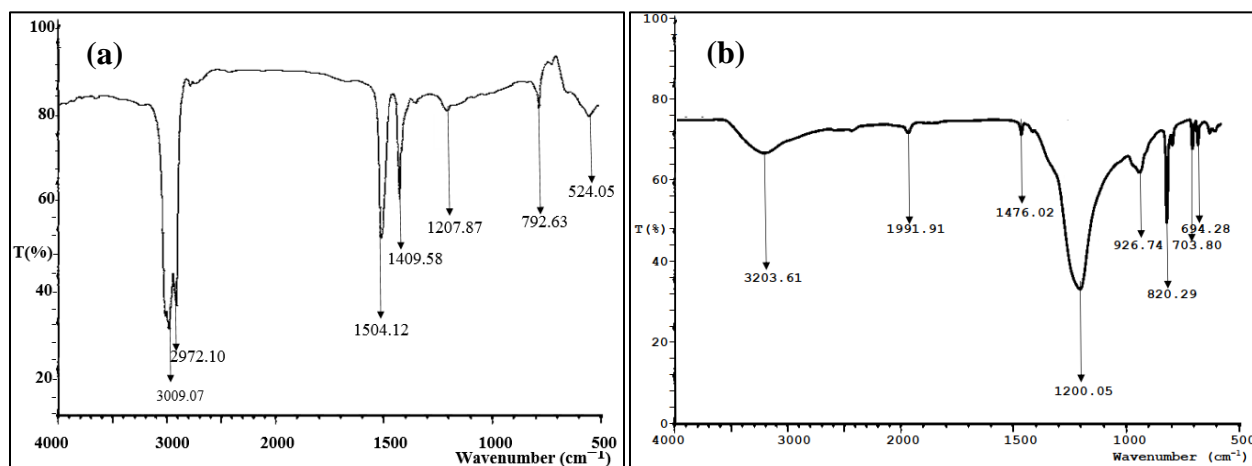


Figure 2: Ce-C composite FTIR spectra obtained before adsorption (a) and after adsorption (b)

3.2.3. Scanning electron micrograph (SEM) analysis result

The surface of the raw Ce-C composite (Fig. 3a) presents a well-defined and underformed structural orientation, with elaborate porosity. The pores are visible as regular openings of clear channels and cavities that suggest a high surface area available for interaction with adsorbates. After adsorption, significant changes were noted in the morphology of the post-adsorption sample (Fig. 3b). Specifically, the surface became more rough and irregular due to adsorption-induced physical changes. Also, the pores are less visible or blocked, indicating that the adsorbates may have occupied the available sites thereby reducing the overall porosity.

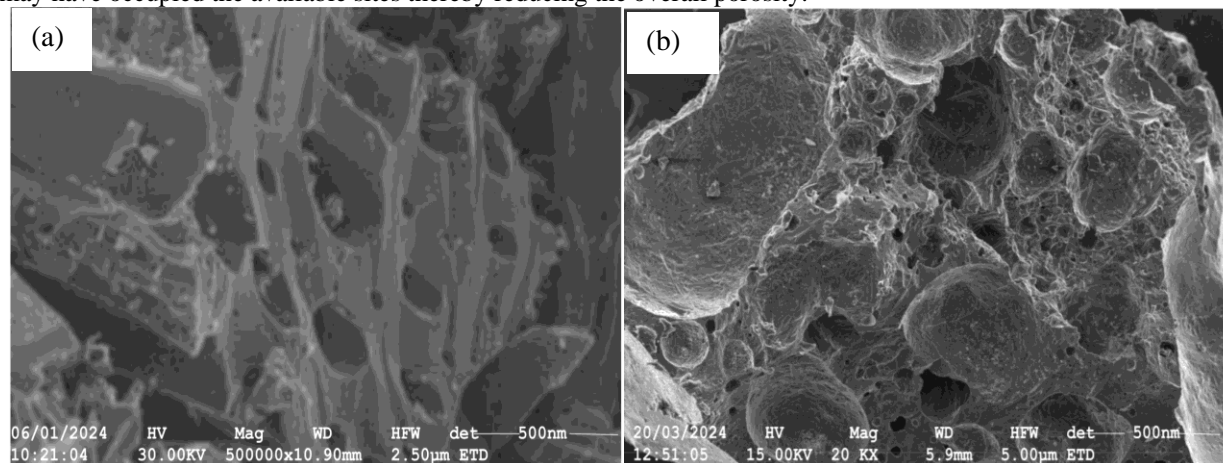


Figure 3: Ce-C composite SEM image obtained before adsorption (a) and after adsorption (b)

3.2.4. X-ray diffraction analysis result

The raw adsorbent sample (Fig. 4a) shows prominent peaks at specific $2\theta^\circ$ values. The most intense peak occurred at $2\theta^\circ = 33.10^\circ$, followed by other significant peaks at 30.01° , 36.3° and 41.5° . The high intensity and sharpness of these peaks indicate a well-defined crystalline structure. After adsorption (Fig. 4b), the peaks show noticeable changes. For instance, the intensity of the peak $2\theta^\circ = 33.10^\circ$ reduced, thus suggesting alterations in the crystalline structure. There are also slight shifts in the positions of the other peaks, indicating changes in lattice parameters due to the adsorption process.

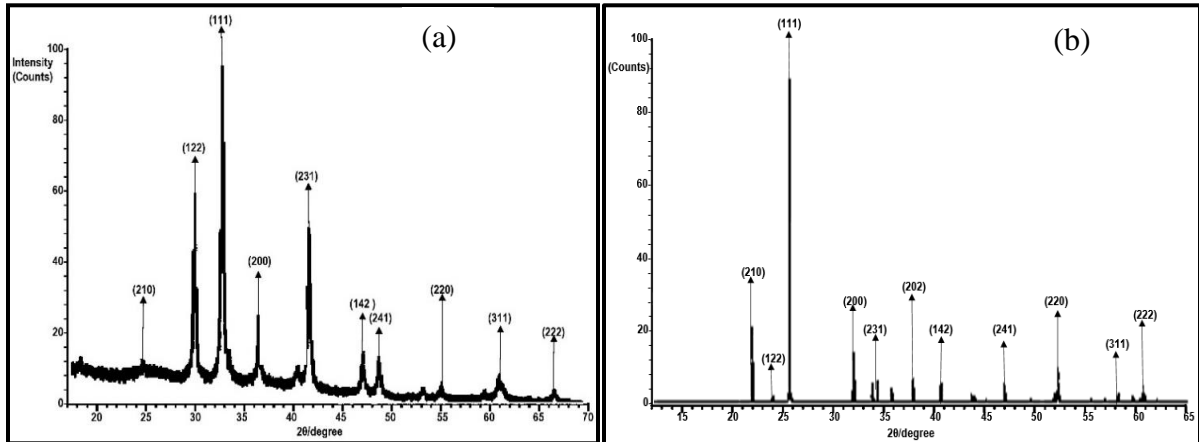


Figure 4: Ce-C composite XRD spectra obtained before adsorption (a) and after adsorption (b)

3.2.5. Thermogravimetric analysis result

The TGA curve (Fig. 5) start at 100% weight at room temperature and shows a steady decrease as the temperature increases. This indicates that the material is losing mass, likely due to decomposition or evaporation of components within the sample. There are notable drops in sample weight at specific temperature ranges: initial weight loss (200-300 °C), major weight loss (300-600 °C) and region of stability (600-800 °C). The DTA curve shows changes in heat flow into or out of the material. Minor fluctuations are observed initially, but there is a significant exothermic peak around 600 °C. The peak at 600 °C suggests a reaction that releases heat, such as crystallization or oxidation.

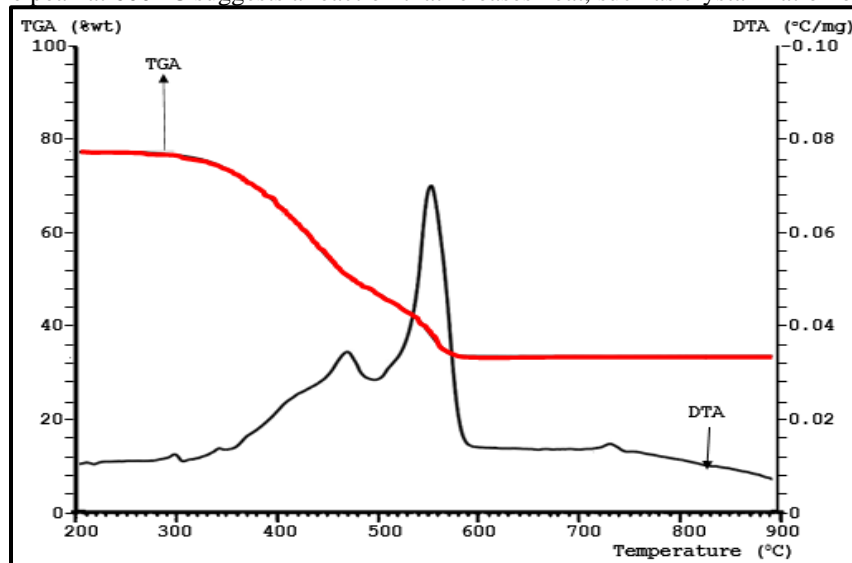


Figure 5: The TGA/DTA spectra for the Ce-C composite

3.3. Batch adsorption studies

3.3.1. Isotherm modeling

The equilibrium values for MET adsorption were analyzed using the Langmuir, Freundlich, and Temkin isotherm models. Figure 6 and Table 2 respectively present the isotherm plots and model-generated parameters. Notably, the Langmuir model, which describes single-layer adsorption on uniform surfaces, provided a maximum adsorption capacity (q_{\max}) of 12.72 mg/g for Ce-C. The separation factor (R_L), calculated as 0.128, indicates that the adsorption process is favourable and spontaneous (Hashem et al., 2024a). For the Freundlich model, which assumes multi-layer adsorption on heterogeneous surfaces, the constant ' n ' was found to be 3.24. Since ' n ' > 1, this suggests that the adsorption is physical rather than chemical (Hashem et al., 2024b). The Temkin model, accounting for adsorbate distribution on heterogeneous sites, yielded a positive b_T -value of 413.15 J/mol, further indicating a favourable adsorption process. All three models had correlation coefficients (R^2) above 0.9, showing that they can all describe the MET adsorption onto Ce-C adsorbents. However, the Langmuir model had the highest R^2 and the lowest chi-square (X^2) values, making it the best fit for the adsorption process.

Table 2: Isotherm model parameters at 40 mg/L initial MET concentration

Langmuir	Freundlich	Temkin
$q_{\max} = 12.72$	$K_F = 4.32$	$K_T = 0.52$
$K_L = 1.13$	$n_F = 3.24$	$b_T = 413.15$
$R_L = 0.128$	Reduced $X^2 = 1.10$	Reduced $X^2 = 0.55$
Reduced $X^2 = 0.39$	$R^2 = 0.92$	$R^2 = 0.96$
$R^2 = 0.97$	Adj. $R^2 = 0.89$	Adj. $R^2 = 0.94$
Adj. $R^2 = 0.96$		

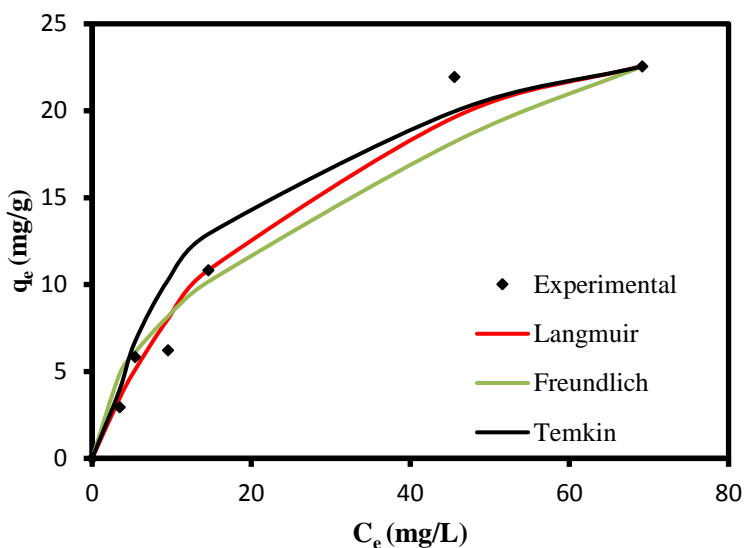


Figure 6: The nonlinear plots generated by the different isotherm models

3.3.2. Kinetic and mechanistic modeling

The obtained kinetic data were used to predict the behaviour of the adsorption process using the kinetic and mechanistic model equations presented in Table 1. The adsorption kinetics graphs for the examined models are shown in Fig. 7, and the corresponding kinetic parameters are presented in Table 3. Notably, the R^2 -value for the PSO model was significantly lower than that of the PFO model (Table 3). The PFO model also exhibited the lowest chi-square (χ^2) value. These findings suggest that the kinetics of MET adsorption onto Ce-C adsorbent is better described by the PFO model.

Additionally, the intra-particle diffusion and Bangham models were employed to investigate the primary solute mass transfer mechanisms during the adsorption of MET onto Ce-C. The intra-particle diffusion and Bangham plots are shown in Figs 7b and 7c, respectively. In this study, the intraparticle diffusion model plot was linear but did not pass through the origin (Fig. 7b). This suggests that the rate-controlling step is not solely governed by intra-particle diffusion (Kurajica et al., 2018). Also, the k_{id} -value was recorded as 0.77 (Table 3), indicating enhanced diffusion.

Analysis of the C-values, which reflect the contribution of intra-particle diffusion, showed negative values, confirming that intra-particle diffusion is the dominant mechanism and plays a critical role in the rate-limiting step, more so than surface or film diffusion (Kurajica et al., 2018; Ofomaja et al., 2020).

Table 3: Kinetic and mechanistic model parameters at 40 mg/L initial concentration

PFO	PSO	IPD	Bangham
$q_e = 14.75$	$q_e = 15.12$	$k_{IPD} = 0.77$	$\alpha = 0.0001$
$k_1 = 0.017$	$k_2 = 0.002$	$C = -1.04$	$k_b = 0.61$
Reduced $X^2 = 0.03$	Reduced $X^2 = 3.18$	Pearson's R = 0.998	Pearson's R = 0.988
$R^2 = 0.991$	$R^2 = 0.834$	$R^2 = 0.997$	$R^2 = 0.953$
Adj. $R^2 = 0.959$	Adj. $R^2 = 0.723$	Adj. $R^2 = 0.994$	Adj. $R^2 = 0.980$

^aPFO: Pseudo-first-order; ^bPSO: pseudo-second-order; ^cIPD: Intraparticle diffusion; ^dBAN: Bangham model

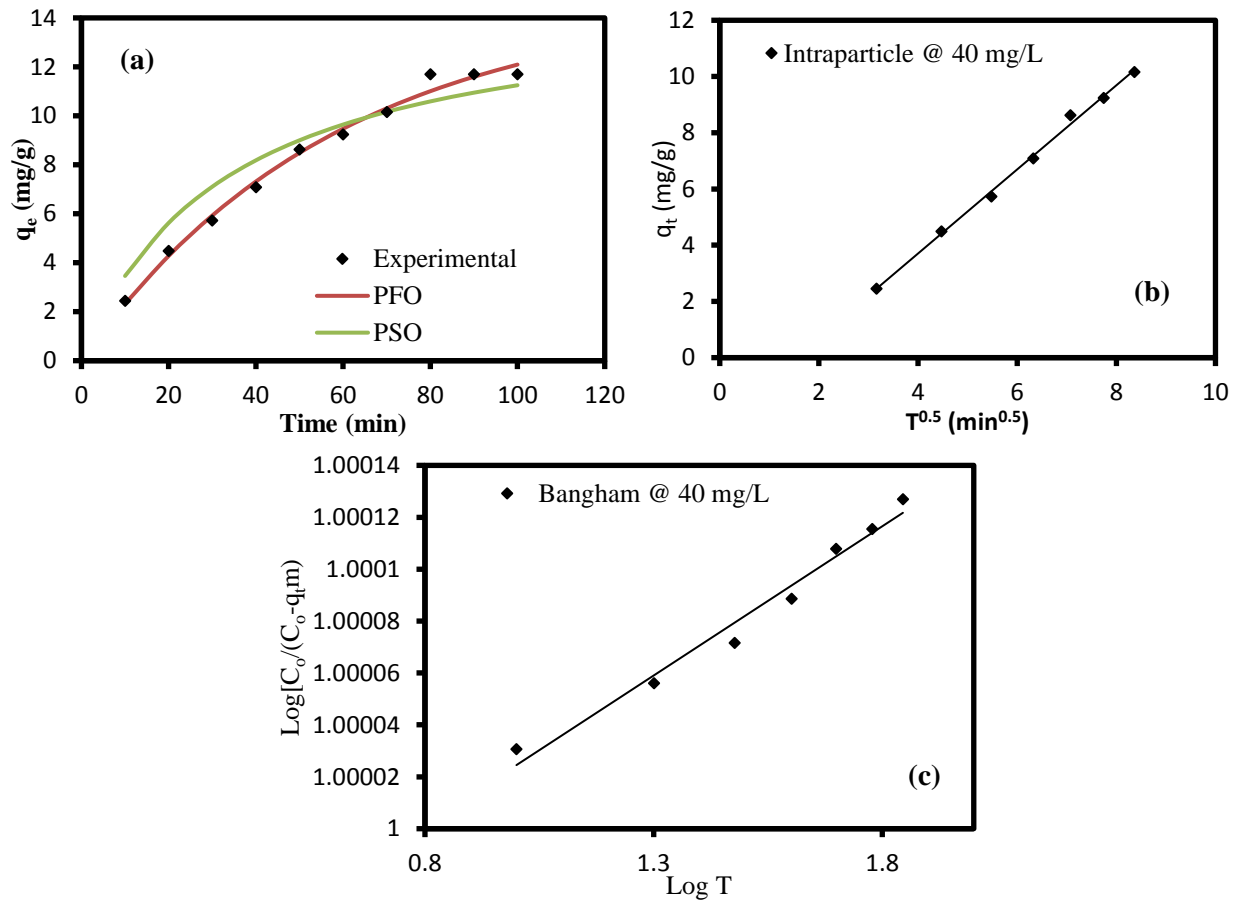


Figure 7: (a) PFO and PSO kinetics (b) intraparticle diffusion and (c) Bangham mechanistic plot

3.4. Thermodynamics studies

At equilibrium, the Van't Hoff reaction isotherm equation correlates the free energy change (ΔG), standard free energy change (ΔG°), and the equilibrium constant (K) at constant temperature (T) using Eq. (9).

$$\Delta G = \Delta G^\circ + RT \ln K \quad (9)$$

When ΔG becomes zero, the Eq. (9) transforms into Eq. (10).

$$\Delta G^\circ = -RT \ln K \quad (10)$$

To predict the standard enthalpy change (ΔH°) and standard entropy change (ΔS°), Eq. (10) is rearranged into Eq. (11).

$$\ln K = \frac{-\Delta G^\circ}{RT} \quad (11)$$

These thermodynamic parameters are related through Eq. (12).

$$\Delta G^{\circ} = \Delta H^{\circ} - T\Delta S^{\circ} \quad (12)$$

Combining Eq. (9) and Eq. (10) leads to the final Van't Hoff shown in Eq. (13).

$$\ln K = \frac{-\Delta H^{\circ}}{RT} + \frac{\Delta S^{\circ}}{R} \quad (13)$$

The values of ΔH° and ΔS° are determined from the slope and intercept of the plot of $\ln K$ vs $1/T$ (Eq. 13).

The thermodynamics of the process were further analyzed by calculating ΔG° , ΔH° , and ΔS° using Eqs. (9) – (13). The negative ΔH° indicates an exothermic process, consistent with the effect of temperature (Hussain et al., 2021). A negative ΔS° suggests a decrease in system entropy (Hashem et al., 2021). Despite the positive ΔG° values (which usually indicate non-spontaneity), the process is still considered spontaneous because ΔH° and ΔS° are both negative and $\Delta H^{\circ} > T\Delta S^{\circ}$ (Hashem et al., 2024b). In another study, the adsorption of methylene blue onto modified kenaf fiber char showed positive ΔH° and ΔS° , indicating an endothermic process with increased randomness at the solid/solution interface (Mahmoud et al., 2012). Although ΔG° was positive at lower temperatures (303 K and 313 K) and negative at 323 K, the adsorption was concluded to be more spontaneous at higher temperatures.

Table 4: Thermodynamic parameters

Temp. (K)	$+\Delta G^{\circ}$ (kJ.mol ⁻¹)	$-\Delta H^{\circ}$ (kJ.mol ⁻¹)	$-\Delta S^{\circ}$ (JK ⁻¹ .mol ⁻¹)
308	5.7097	62.2736	218.0317
313	5.8877		
318	6.4248		
323	7.2394		
328	8.8645		
333	11.5198		

4. Conclusion

This study successfully developed a cellulose-chitosan composite (Ce-C) for the adsorption of metronidazole (MET) from water. The composite was characterized and its adsorption performance was tested under various conditions. Results showed the Ce-C composite has a high adsorption capacity, fast kinetics, and works effectively even at low MET concentrations. The Langmuir isotherm model fit the data best, indicating monolayer adsorption on a homogeneous surface. The adsorption process was exothermic and spontaneous, and the composite's mesoporous structure facilitated MET adsorption. Intraparticle diffusion was identified as the dominant adsorption mechanism. Due to the ongoing issue of antibiotic contamination, the Ce-C composite offers a cost-effective and sustainable solution for removing MET and potentially other pharmaceutical pollutants. Future research could explore scaling up production and testing the composite in real-world wastewater systems.

References

- Abd El-Monaem, E. M., Eltaweil, A. S., Elshishini, H. M., Hosny, M., Abou Alsoaud, M. M., Attia, N. F., El-Subruiti, G. M., & Omer, A. M. 2022. Sustainable adsorptive removal of antibiotic residues by chitosan composites: An insight into current developments and future recommendations. *Arabian Journal of Chemistry*, 15(5), 103743.
- Aniagor, C. O., Aly, A., Mohamed, L. A., & Hashem, A. 2024. Removal of Methylene blue dye from contaminated wastewater using lignocellulosic biomasses: A comparative study. *Waste Management Bulletin*, 2(2), 213-225.
- Aniagor, C. O., Taha, G. M., Badawy, S. M., El-Naggar, M. E., & Hashem, A. 2022. Preparation of a novel acrylic fiber-based hydrogel and its utilization for the removal of aqueous lead ion. *Journal of Materials Research and Technology*, 18, 1450-1459.
- Barus, D. A., Humaidi, S., Ginting, R. T., & Sitepu, J. 2022. Enhanced adsorption performance of chitosan/cellulose nanofiber isolated from durian peel waste/graphene oxide nanocomposite hydrogels. *Environmental nanotechnology, monitoring & management*, 17, 100650.
- Binh, V. N., Dang, N., Anh, N. T. K., & Thai, P. K. 2018. Antibiotics in the aquatic environment of Vietnam: sources, concentrations, risk and control strategy. *Chemosphere*, 197, 438-450.
- Chan, K., Morikawa, K., Shibata, N., & Zinchenko, A. 2021. Adsorptive removal of heavy metal ions, organic dyes, and pharmaceuticals by dna-chitosan hydrogels. *Gels*, 7(3), 112.
- Feng, Z., Zhai, X., & Sun, T. 2022. Sustainable and efficient removal of paraben, oxytetracycline and metronidazole using magnetic porous biochar composite prepared by one step pyrolysis. *Separation and Purification Technology*, 293, 121120.

- Ferrah, N., Merghache, D., Meftah, S., & Benbellil, S. 2022. A new alternative of a green polymeric matrix chitosan/alginate-polyethyleniminemethylene phosphonic acid for pharmaceutical residues adsorption. *Environmental Science and Pollution Research*, 29(9), 13675-13687.
- Gong, Y., Liu, L., Wang, F., Pei, Y., Liu, S., Lyu, R., & Luo, X. 2021. Aminated chitosan/cellulose nanocomposite microspheres designed for efficient removal of low-concentration sulfamethoxazole from water. *Journal of Molecular Liquids*, 339, 116407.
- Hashem, A., Abou-Okeil, A., Fikry, M., Aly, A., & Aniagor, C. O. 2021. Isotherm and Kinetics Parametric Studies for Aqueous Hg(II) Uptake onto N-[2-(Methylamino)Ethyl]Ethane-1,2-Diaminated Acrylic Fibre. *Arabian Journal for Science and Engineering*. doi:<https://doi.org/10.1007/s13369-021-05416-x>
- Hashem, A., Aniagor, C. O., Farag, S., Fikry, M., Aly, A., & Amr, A. 2024a. Evaluation of the adsorption capacity of surfactant-modified biomass in an aqueous acid blue 193 system. *Waste Management Bulletin*, 2(1), 172-183.
- Hashem, A., Aniagor, C. O., Mohamed, L., Abdellah, E. M., Morsy, O., & Aly, A. 2024b. Peach seed shell and *Aspergillus oryzae* as adsorbents for the uptake of acid violet 90 dye from wastewater. *Sustainable Chemistry for the Environment*, 100115.
- Hejna, M., Kapuścińska, D., & Aksmann, A. 2022. Pharmaceuticals in the aquatic environment: A review on ecotoxicology and the remediation potential of algae. *International Journal of Environmental Research and Public Health*, 19(13), 7717.
- Hussain, S., Kamran, M., Khan, S. A., Shaheen, K., Shah, Z., Suo, H., Khan, Q., Shah, A. B., Rehman, W. U., & Al-Ghamdi, Y. O. 2021. Adsorption, kinetics and thermodynamics studies of methyl orange dye sequestration through chitosan composites films. *International journal of biological macromolecules*, 168, 383-394.
- Iber, B. T., Kasan, N. A., Torsabo, D., & Omuwa, J. W. 2022. A review of various sources of chitin and chitosan in nature. *Journal of Renewable Materials*, 10(4), 1097.
- Inyinbor, A. A., Bello, O. S., Fadiji, A. E., & Inyinbor, H. E. 2018. Threats from antibiotics: A serious environmental concern. *Journal of Environmental Chemical Engineering*, 6(1), 784-793.
- Khan, A. H. A., & Barros, R. 2023. Pharmaceuticals in Water: Risks to Aquatic Life and Remediation Strategies. *Hydrobiology*, 2(2), 395-409.
- Koch, N., Islam, N. F., Sonowal, S., Prasad, R., & Sarma, H. 2021. Environmental antibiotics and resistance genes as emerging contaminants: methods of detection and bioremediation. *Current research in microbial sciences*, 2, 100027.
- Kumar, A., Patra, C., Rajendran, H. K., & Narayanasamy, S. 2022. Activated carbon-chitosan based adsorbent for the efficient removal of the emerging contaminant diclofenac: synthesis, characterization and phytotoxicity studies. *Chemosphere*, 307, 135806.
- Kumar, P. S., Ramalingam, S., Senthamarai, C., Niranjanaa, M., Vijayalakshmi, P., & Sivanesan, S. 2010. Adsorption of dye from aqueous solution by cashew nut shell: Studies on equilibrium isotherm, kinetics and thermodynamics of interactions. *Desalination*, 261(1-2), 52-60.
- Kurajica, S., Minga, I., Blazic, R., Muzina, K., & Tominac, P. 2018. Adsorption and degradation kinetics of methylene blue on as-prepared and calcined titanate nanotubes. *Athens J. Sci*, 5, 7-22.
- Liu, Y., Nie, P., & Yu, F. 2021. Enhanced adsorption of sulfonamides by a novel carboxymethyl cellulose and chitosan-based composite with sulfonated graphene oxide. *Bioresource technology*, 320, 124373.
- Luo, X., Liu, L., Wang, L., Liu, X., & Cai, Y. 2019. Facile synthesis and low concentration tylosin adsorption performance of chitosan/cellulose nanocomposite microspheres. *Carbohydrate polymers*, 206, 633-640.
- Mahmoud, D. K., Salleh, M. A. M., Karim, W. A. W. A., Idris, A., & Abidin, Z. Z. 2012. Batch adsorption of basic dye using acid treated kenaf fibre char: Equilibrium, kinetic and thermodynamic studies. *Chemical Engineering Journal*, 181, 449-457.
- Mashile, P. P., & Nomngongo, P. N. 2021. Magnetic cellulose-chitosan nanocomposite for simultaneous removal of emerging contaminants: Adsorption kinetics and equilibrium studies. *Gels*, 7(4), 190.
- Merino, D., & Athanassiou, A. 2023. Alkaline hydrolysis of biomass as an alternative green method for bioplastics preparation: In situ cellulose nanofibrillation. *Chemical Engineering Journal*, 454, 140171.
- Mohamed, L. A., Aniagor, C. O., & Hashem, A. 2021. Isotherms and kinetic modelling of mycoremediation of hexavalent chromium contaminated wastewater. *Cleaner Engineering and Technology*, 4, 100192. doi:<https://doi.org/10.1016/j.clet.2021.100192>
- Naebe, M., Li, Q., Onur, A., & Denning, R. 2016. Investigation of chitosan adsorption onto cotton fabric with atmospheric helium/oxygen plasma pre-treatment. *Cellulose*, 23, 2129-2142.
- Nordin, A. H., Ngadi, N., Ilyas, R. A., Abd Latif, N. A. F., Nordin, M. L., Mohd Syukri, M. S., Nabgan, W., & Paiman, S. H. 2023. Green surface functionalization of chitosan with spent tea waste extract for the

- development of an efficient adsorbent for aspirin removal. *Environmental Science and Pollution Research*, 30(60), 125048-125065.
- Oba, S. N., Ighalo, J. O., Aniagor, C. O., & Igwegbe, C. A. 2021. Removal of ibuprofen from aqueous media by adsorption: A comprehensive review. *Science of the total environment*, 146608. doi:<https://doi.org/10.1016/j.scitotenv.2021.146608>
- Ofomaja, A. E., Naidoo, E. B., & Pholosi, A. 2020. Intraparticle diffusion of Cr (VI) through biomass and magnetite coated biomass: A comparative kinetic and diffusion study. *South African Journal of Chemical Engineering*, 32(1), 39-55.
- Papageorgiou, M., Maroulas, K. N., Evgenidou, E., Bikiaris, D. N., Kyzas, G. Z., & Lambropoulou, D. A. 2024. Simultaneous Removal of Seven Pharmaceutical Compounds from a Water Mixture Using Modified Chitosan Adsorbent Materials. *Macromol*, 4(2), 304-319.
- Ramadhani, P., Chaidir, Z., Zilfa, Z., Fauzia, S., & Zein, R. 2021 Isolation of chitosan from shrimp shell (*Metapenaeus monoceros*) as adsorbent for removal of metanil yellow dyes. *Journal of the Iranian Chemical Society*, 1-15.
- Szentmihályi, K., Klébert, S., May, Z., Bódis, E., Mohai, M., Trif, L., Feczko, T., & Károly, Z. 2022. Immobilization of Metronidazole on Mesoporous Silica Materials. *Pharmaceutics*, 14(11), 2332.
- Wang, B.-T., Hu, S., Yu, X.-Y., Jin, L., Zhu, Y.-J., & Jin, F.-J. 2020. Studies of cellulose and starch utilization and the regulatory mechanisms of related enzymes in fungi. *Polymers*, 12(3), 530.